Articles

Conformations of Nucleoside Analogue 1-(2′-Deoxy-β-D-ribofuranosyl)-1,2,4-triazole-3-carboxamide in Different DNA Sequence Contexts†

Douglas A. Klewer,‡ Peiming Zhang,§,|| Donald E. Bergstrom,§,⊥ V. Jo Davisson,⊥ and Andy C. LiWang*,‡

Department of Biochemistry and Biophysics, Texas A&M University, College Station, Texas 77843-2128, Department of Medicinal Chemistry and Molecular Pharmacology, Purdue University, West Lafayette, Indiana 47907, and Walther Cancer Institute Indianapolis, Indiana 46208

Received June 26, 2000; Revised Manuscript Received November 28, 2000

ABSTRACT: The concept of using a dynamic base-pairing nucleobase as a mode for degenerate recognition presents a unique challenge to analysis of DNA structure. Proton and phosphorus NMR studies are reported for two nine-residue DNA oligodeoxyribonucleotides, d(CATGGGTAC)·d(GTAC**N**CATG) (**1**) and d(CATGTGTAC)·(GTAC**N**CATG) (**2**), which contained 1-(2′-deoxy-β-D-ribofuranosyl)-1,2,4-triazole-3-carboxamide (**N**) in the center of the helix at position 14. The duplexes were compared to the canonical Watson−Crick duplexes, d(CATGGGTAC)·d(GTACCCATG) (**3**) and d(CATGTGTAC)·d(GTACACATG) (**4**). Two-dimensional NOESY spectra of **1**−**4** in H_2O and D_2O solutions collected at 5 °C allowed assignment of the exchangeable and nonexchangeable protons for all four oligodeoxyribonucleotides. Thermodynamic and circular dichroism data indicated that **1**−**4** formed stable, B-form duplexes at 5 °C. Two-dimensional ^1H-^{31}P correlation spectra indicated that there were minor perturbations in the backbone only near the site of the triazole base. Strong NOESY cross-peaks were observed between the H5 and H1′ of **N**14 in **1** and, unexpectedly, **2**, which indicated that, in both duplexes, **N**14 was in the syn_χ conformation about the glycosidic bond. NOESY spectra of **1** and **2** recorded in 95% H_2O, 5% D_2O indicated that the imino proton of the base opposite **N**14, G5, or T5, formed a weak hydrogen bond with **N**14. These conformations place the polar carboxamide functional group in the major groove with motional averaging on the intermediate time scale.

Nucleic acid base analogues that can base pair with the four DNA[1] bases with equal affinity would be useful as wild cards in the design of oligodeoxyribonucleotide hybridization probes. The search for such a universal base has been intensive in recent years (*1*−*11*). Recently, a family of azole carboxamide nucleotide analogues has been developed that were proposed to enable base pairing with the four naturally occurring nucleobases through simple bond rotations (*3*, *12*−*18*). A great deal is known about the thermodynamic and enzymatic parameters that characterize how these azole bases interact with the natural bases. For example, thermodynamically, DNA duplexes that contain imidazole-4-carboxamide are most stable when the imidazole is paired with T or G (T > G > A > C) (*15*). The dynamic aspects of this structural model require an approach such as NMR spectroscopy for analysis.

A detailed analysis of the structural features of a modified base inserted into a DNA duplex opposite different bases may lead to a greater understanding of how modified bases behave in different sequence contexts. The nucleoside analogue 1-(2′-deoxy-β-D-ribofuranosyl)-1,2,4-triazole-3-carboxamide (hereafter referred to as **N**) was designed such that it could mimic the hydrogen-bonding patterns of all four canonical bases as shown in Figure 1 through rotations about the two torsion angles χ and τ. However, thermodynamic experiments have shown that the G:**N** base pair is the most stable (G:**N** > T:**N** ≈ A:**N** > C:**N** ≈ **N**:**N**) (*19*). The differences in stability prompted us to investigate the conformations of **N** in two different sequence contexts. **N** was incorporated into d(CATGGGTAC)·d(GTAC**N**CATG) (**1**) and d(CATGTGTAC)·d(GTAC**N**CATG) (**2**) to determine

† Funding was provided by the National Institutes of Health grants GM61398-01 (A.C.L.) and GM53155 (D.E.B./V.J.D.), and the NMR instrumentation in the Biomolecular NMR Laboratory at Texas A&M University was supported by a grant from the National Science Foundation (DBI-9970232).

* To whom correspondence should be addressed. Phone: (979) 862-6952. Fax: (979) 845-9274. E-mail: andy-liwang@tamu.edu.

‡ Department of Biochemistry and Biophysics.

§ Walther Cancer Institute.

|| Present Address: Motorola, Biochips Systems, Phoenix Research and Development Center, 2100 East Elliot Road, M/D AZ34/EL623, Tempe, AZ 85284.

⊥ Department of Medicinal Chemistry and Molecular Pharmacology.

[1] Abbreviations: NOE, nuclear Overhauser effect; NOESY, nuclear Overhauser enhancement spectroscopy; ppm, parts per million; DNA, deoxyribonucleic acid; EDTA, ethylenediaminetetraacetic acid; CD, circular dichroism; T_m, melting temperature; T, tesla; DSS, sodium 2,2-dimethyl-2-silapentane-5-sulfonate.

10.1021/bi001448f CCC: $20.00
Published on Web 01/19/2001

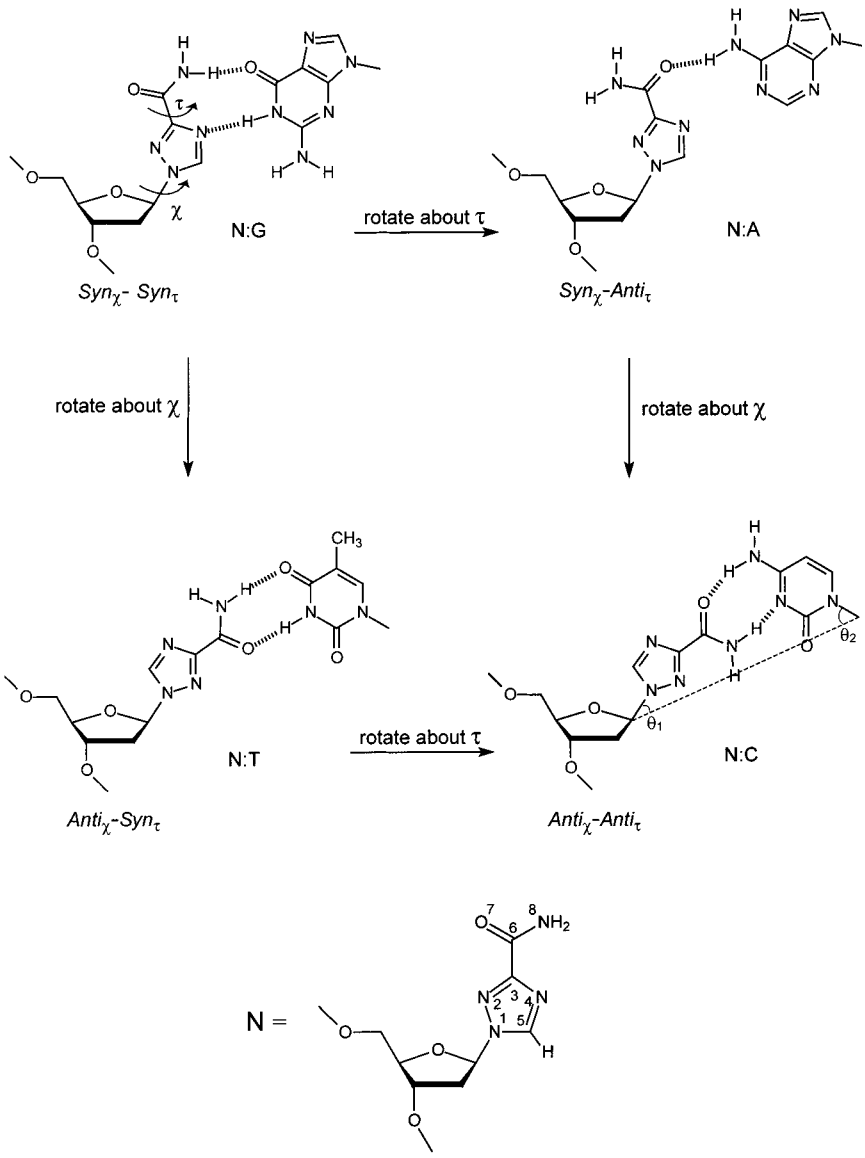

FIGURE 1: Illustration of the predicted orientations and hydrogen bonding of 1,2,4-triazole-3-carboxamide (**N**), when opposite A, G, C, and T, due to rotations around the glycosidic bond, χ, and the exocyclic carboxamide bond, τ. The torsion angles χ and τ are defined as O4′−C1′−N1−N2 and N2−C4−C6−O8, respectively. The dashed line in the illustration of the anti$_\chi$−anti$_\tau$ conformation denotes the interstrand C1′ to C1′ distance and the angles θ_1 and θ_2.

the behavior of its local conformation when opposite G or T and to assess the molecular models that predicted two conformations about the glycosidic bond (*15*). Duplexes d(CATGGGTAC)·d(GTACCCATG) (**3**) and d(CATGTGTAC)·d(GTACACATG) (**4**) were also investigated for comparison to **1** and **2**, respectively. The NMR data allow for the determination of the type of base pairs formed, the handedness of the double helix, the glycosidic torsion angle, whether bases were stacked within the helix, and perturbation of the backbone.

EXPERIMENTAL PROCEDURES

Oligodeoxyribonucleotides. Nine-residue oligodeoxyribonucleotides d(CATGXGTAC) and d(GTACYCATG), where X is G or T and Y is C, A, or **N**, were synthesized on a 10 μmol scale by standard β-cyanoethylphosphoramidite chemistry in the Laboratory for Macromolecular Structure at Purdue University, West Lafayette, Indiana. Purification of the oligodeoxyribonucleotides was accomplished by trityl-on purification on a 900 mg C18 cartridge (Alltech) which was preconditioned with 2 M triethylammonium acetate. The failure sequences were removed by elution with water, the trityl groups were removed by flushing the cartridge with 3% trifluoroacetic acid, and the desired oligodeoxyribonucleotide was eluted with 20% aqueous acetonitrile. The oligodeoxyribonucleotides were converted to the sodium form with Dowex 50W-4X ion-exchange resin (Aldrich) and lyophilized to dryness. Purity was determined by reversed-phase HPLC (PRP-1, Hamilton) and MALDI mass spectrometry. The synthesis of the phosphoramidite of **N** is described elsewhere (*19*).

Circular Dichroism. Circular dichroism spectropolarimitry (CD) was used to ascertain the average conformation of each duplex. Spectra were recorded at 5 °C on an AVIV 62DS spectro-polarimiter. Ten scans between 220 and 320 nm were averaged with a bandwidth of 1 nm and a 1.0 s averaging time. Approximately 0.1 mM duplex was dissolved in buffer (100 mM NaCl, 10 mM Na_2HPO_4, and 0.5 mM EDTA, pH

7.0) in a 1 mm quartz cuvette.

Thermal Denaturation. The T_m data were collected on a Cary 1 spectrophotometer equipped with a temperature controller and a six-cell sample changer. Data were collected for DNA duplexes at five different concentrations (2, 4, 8, 16, and 30 μM) in 100 mM NaCl, 10 mM Na_2HPO_4, 0.5 mM EDTA buffer at pH 7. Capped cuvettes with 10 mm path lengths were used. The samples were heated to 65 °C for 15 min, cooled slowly to room temperature, and equilibrated at 2 °C for 30 min. The temperature was increased to 98 °C, and the percent transmittance at 260 and 280 nm was recorded every 0.3 °C. The temperature was measured by inserting a thermocouple into a cuvette that contained only buffer. Thermodynamic parameters were extracted from the melting profiles by nonlinear least-squares parameter estimation with the program t-melt as described elsewhere (*20*).

Sample Preparation. A 1:1 ratio of complimentary strands was accomplished by titration of one strand with the other at 80 °C in 99.99% D_2O while monitoring the relative aromatic peak intensities with one-dimensional ^{1}H NMR. This was performed quickly to minimize H/D exchange of purine H8 protons for deuterons (*21*). The solutions were then freeze-dried, redissolved in 300 μL of aqueous buffer (100 mM NaCl, 10 mM Na_2HPO_4, and 0.5 mM EDTA, pH 7), and annealed by placing the samples in a 4 L water bath at 80 °C and allowing the bath to slowly cool to 4 °C. The buffered solutions were then lyophilized and redissolved in 300 μL of either 99.996% D_2O or 5% D_2O in H_2O for a final duplex concentration of approximately 3 mM.

NMR Spectroscopy. NMR spectra were collected at the Biomolecular NMR Laboratory at Texas A&M University on an 11.7 T Varian Inova spectrometer. All spectra were collected at 5 °C and referenced internally to sodium 2,2-dimethyl-2-silapentane-5-sulfonate (DSS). Two-dimensional NOESY spectra of samples dissolved in 99.996% D_2O were collected as 1024 × 1024 matrixes with corresponding acquisition times of 170.5 ms in the t_1 and t_2 dimensions. The mixing time was 120 ms and the relaxation delay was 3 s. The total acquisition time per spectrum was 31 h. The final digital resolution in the F_1 and F_2 dimensions was 2.93 Hz/pt. Solvent suppression during acquisition of NOESY spectra of samples in 5% D_2O/95% H_2O was accomplished using the WATERGATE sequence (*22*). H_2O NOESY spectra were collected at mixing times of 200 and 90 ms as 768 × 1536 matrixes with corresponding acquisition times of 69.8 and 139.6 ms in the t_1 and t_2 dimensions, respectively. The final digital resolutions in the F_1 and F_2 dimensions were 7.16 and 3.58 Hz/pt, respectively. The total acquisition time per spectrum was 25.6 h.

One-dimensional ^{31}P spectra were recorded with a spectral width of 1500 Hz and an acquisition time of 192 ms. The relaxation delay was 1.0 s, the number of transients was 8192, and the total time of the experiment was 2.7 h. A line broadening function of 1.0 Hz was applied and the FID was zero-filled to 1024 prior to Fourier transformation. The resulting digital resolution was 1.46 Hz. Two-dimensional ^{1}H-^{31}P spectra were recorded with the nonconstant time pulse sequence described by Bax and co-workers (*23*). Samples dissolved in 99.996% D_2O were collected as 104 × 512 matrixes with corresponding acquisition times of 128.3 ms and 127.9 ms in the t_1 and t_2 dimensions, respectively. The number of transients per t_2 increment was 256, and the total acquisition time per spectrum was 25.3 h. The final digital resolution in the F_1 and F_2 dimensions was 1.58 and 1.95 Hz, respectively.

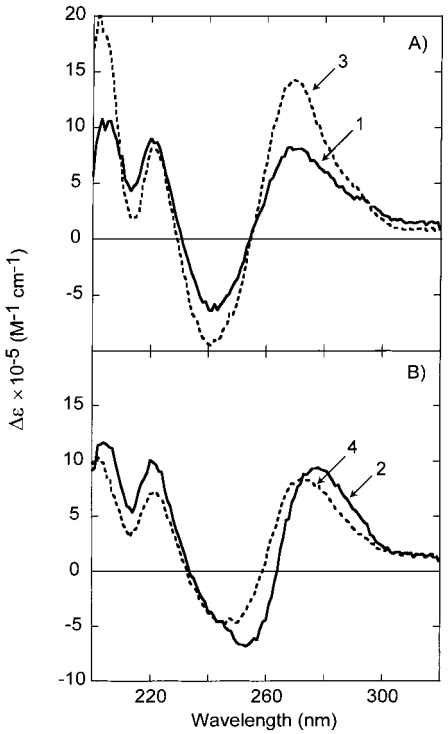

FIGURE 2: Circular dichroism spectra of 0.1 mM duplexes **1**−**4** at 5 °C. (A) The solid line is the spectrum of duplex **1**, d(CATGG-GTAC)·d(GTAC**N**CATG), and the dashed line is the spectrum of duplex **3**, d(CATGGGTAC)·d(GTACCCATG). (B) The solid line is the spectrum of duplex **2**, d(CATGTGTAC)·(GTAC**N**CATG), and the dashed line is the spectrum of duplex **4**, d(CATGTGTAC)·d(GTACACATG). The spectra were not corrected for the small differences in concentration.

Computational Methods. All calculations were carried out with the Gaussian 94 software at Purdue University as previously described (*15*).

RESULTS

Optical Data. The four duplexes in this study differ only at residue 14. Oligodeoxyribonucleotides **1** and **2** contain **N** at position 14 while **3** and **4** contain C and A, respectively. Circular dichroism spectra (Figure 2) were collected at 5 °C to determine the average conformation of the oligodeoxyribonucleotides in solution. The CD spectra of sequences **1** and **3** have maxima at about 270 nm and minima at about 240 nm (Figure 2A). The spectra for **2** and **4** are shown in Figure 2B. Oligodeoxyribonucleotide **4** has extrema similar to **1** and **3**, a maximum at 270 nm and a minimum at 245 nm. Oligodeoxyribonucleotide **2** shows a small shift of the maximum and minimum to 277 and 252 nm. The CD spectra show that oligodeoxyribonucleotides **1**−**4** exist in solution at 5 °C as B-form duplexes. The spectra of **1** and **3** are very similar, as are those of **2** and **4**. This indicates that the presence of **N** has a small effect on the overall conformation of the duplex.

UV-melting profiles were carried out to determine the stability of the duplexes. The melting curves (data not shown) show a hyperchromic shift that is typical of the duplex to random-coil transition of DNA with a single inflection at

Table 1: Melting Temperatures and Thermodynamic Parameters of d(CATGXGTAC)·(GTACYCATG)[a]

X−Y	T_m (°C)[b]	$-\Delta H°$ (kcal mol^{-1})	$-\Delta S°$ (cal mol^{-1} K^{-1})	$-\Delta G°_{25}$ (kcal mol^{-1})
G−C	41	63 ± 2	179 ± 7	9.4 ± 0.1
G−**N**	25	61 ± 2	184 ± 6	6.3 ± 0.1
T−A	38	59 ± 6	168 ± 21	8.7 ± 0.1
T−**N**	22	58 ± 3	174 ± 10	5.6 ± 0.1

[a] Thermodynamic values were obtained from van't Hoff analysis of experiments carried out on **1**−**4** in as described elsewhere (*20*). See text for details. The error in the standard free energy $\Delta G°_{25}$ was calculated according to the method of Turner (*46*). [b] The T_m values were calculated from the thermodynamic data at a concentration of 10^{-4} M. The errors in the measured T_m values were ±1 °C

the melting point (T_m). Van't Hoff plots (Supporting Information) of the T_m data show a linear relationship which indicates a two-state melting transition for all four duplexes. Table 1 lists the thermodynamic parameters calculated from least-squares fits of the van't Hoff data. Replacing a canonical base with **N** decreased the duplex stability by approximately 3 kcal/mol ($\Delta\Delta G°_{25}$ for **1** to **3** is 3.2 ± 0.1 kcal/mol and for **2** to **4** it is 3.1 ± 0.1 kcal/mol). Thus, the extent of the destabilization upon substitution with **N** is not dependent on whether the opposing base is a G or T.

Nonexchangeable Protons. The nonexchangeable base and sugar protons of all four duplexes were assigned with the 2D NOESY spectra recorded in 99.996% D_2O. These resonances were subsequently used to assign the additional peaks of the NOESY spectra recorded in 95% H_2O. Figure 3 shows the chemical shift connectivities between the aromatic protons (7.0−8.5 ppm) and the H1′ and cytidine H5 (and labile cytosine H4) (*24*) protons (5.2−6.4 ppm) in duplex **1** (A) and **2** (B). All purine H8 and pyrimidine H6 protons show NOESY cross-peaks with the H1′ protons on the same residue and on the sugar on the 5′ side, which is typical for A- and B-form DNA (*25*−*27*). Tracing along the connectivities established the assignments of all of the base and H1′ protons for each strand. This same procedure was then used to assign the H2′, H2″, H3′, and H4′ protons (data not shown). The stereospecific assignment of the H2′ and H2″ protons was based on the stronger H1′ to H2″ cross-peak intensities, relative to those of the H1′ to H2′ cross-peaks, in short mixing time (30 ms) NOESY spectra. The H2 of A8 and A12 have weak interstrand NOEs with the H1′ of A12 and A8, respectively, and helped establish the duplex nature of the oligonucleotides.

Glycosidic Bond Angle of N14. The absence of a NOESY cross-peak between the H5 of **N**14 and the H1′ of C13 and the presence of cross-peaks between H5 of **N**14 and H5 of C15 in **1** and **2** indicated that for both duplexes the glycosidic torsion angles, χ, of **N**14 were within the +sc-syn conformational regime (*24*). The NOESY cross-peak between H5 of **N**14 and H5 of C15 was stronger in **1** than **2** and indicated that the χ angle of **N**14 of **1** was, on average, closer to syn than that of **2.** A NOESY cross-peak between H5 of **N**14 and H41 of C15 in **1**, which was not observed in the spectrum of **2**, was further evidence that the χ angle of **1** was closer to the syn conformation (Figure 3). While the intensity of the cross-peak of H5 of **N**14 with its own H1′ in **1** was comparable to those between the H5 and H6 protons of the cytosine bases, the corresponding cross-peak of **N**14 of **2** was broadened, most likely by conformational exchange.

Phosphorus NMR. The majority of the 16 backbone phosphate resonances of **1**−**4** was dispersed between −3.6 and −4.7 ppm and was characteristic of an unperturbed phosphodiester backbone (Supporting Information). However, **1** and **2** displayed resonances that were shifted downfield relative to the unmodified duplexes. The spectrum of **1** had a peak at −3.14 ppm, and the spectrum of **2** had a peak at −3.49 ppm. Chemical shift assignments of the downfield-shifted ^{31}P resonances were accomplished with 2D ^{1}H-^{31}P correlation spectra (Figure 4). Spectral crowding prevented the unambiguous assignment of all of the backbone phosphates. In duplex **1**, the phosphate at −3.14 ppm was coupled to a H3′ proton at 4.97 ppm, which was the chemical shift of the H3′ of G5 and **N**14; the phosphate at −3.14 ppm could be either that of G6 or C15. In duplex **2**, the phosphate at −3.49 ppm was coupled to a H3′ proton resonating at 4.89 ppm, which was the chemical shift of H3′ of T7 and C15; the 5′-phosphate could be either that of A8 or A16.

Labile Protons. Assignment of the labile amino and imino protons was accomplished with NOESY spectra recorded at 5 °C in 95% H_2O and 5% D_2O. The amino protons of cytidine residues were assigned from strong, intraresidue NOESY cross-peaks between the hydrogen bonded (H41), non-hydrogen bonded (H42), and H5 protons of the cytidine base (Figure 3). The amino protons of the guanosine residues were not observed in our spectra, which is normal for DNA duplexes. Figure 3A also shows weak cross-peaks between the amide protons (H81 and H82) of **N**14 and the H5 protons of C13 and C15 of **1**. The amide protons of **N**14 in duplex **1** resonate at 8.16 and 7.10 ppm. However, the NOESY spectra of **2** in H_2O do not contain any cross-peaks that could be attributed to the amide protons of **N**14 (Figure 3B).

Figures 5 and 6 show expanded contour plots of the imino region of the NOESY spectrum (200 ms mixing time) of **1** and **2**. The through-space connectivities between the imino (10.2−14 ppm) and the amino and aromatic protons (6.0−8.5 ppm) are shown in Figures 5A and 6A and the connectivities between imino protons are shown in Figures 5B and 6B. Interstrand cross-peaks between the thymidine imino and adenosine H2 and amino protons were observed for each of the four A:T base pairs. Cross-peaks between the guanosine imino protons and the cytidine amino protons were observed for each G:C base pair except for C1:G18, which was at the end of the duplex. These results established that **1** and **2** formed stable duplexes at 5 °C and all A:T and G:C base pairs of **1** and **2** (and **3** and **4**, data not shown) formed stable Watson-Crick base pairs with the exception of C1:G18, which was at the termini of the duplexes. In addition, interstrand imino−imino cross-peaks were observed between T3 and T17 and T7 and T11 (Figures 5B and 6B).

The imino proton of G5 of **1** resonated at 10.47 ppm, which was about 2.5 ppm upfield from the other guanosine imino resonances. The assignment was based upon NOESY cross-peaks between the imino proton of G5 and the imino protons of G4 and G6 (Figure 5B). The imino proton of G5 also produced NOEs with the H41 and H42 protons of C13 (Figure 5A) and an amide proton of **N**14 (Figure 5A). This established that the imino proton of G5 was directed toward the amide proton of **N**14 and oriented toward the interior of the helix.

The imino proton of T5 of **2** resonated at 11.36 ppm, which was about 3 ppm upfield from the other thymidine imino

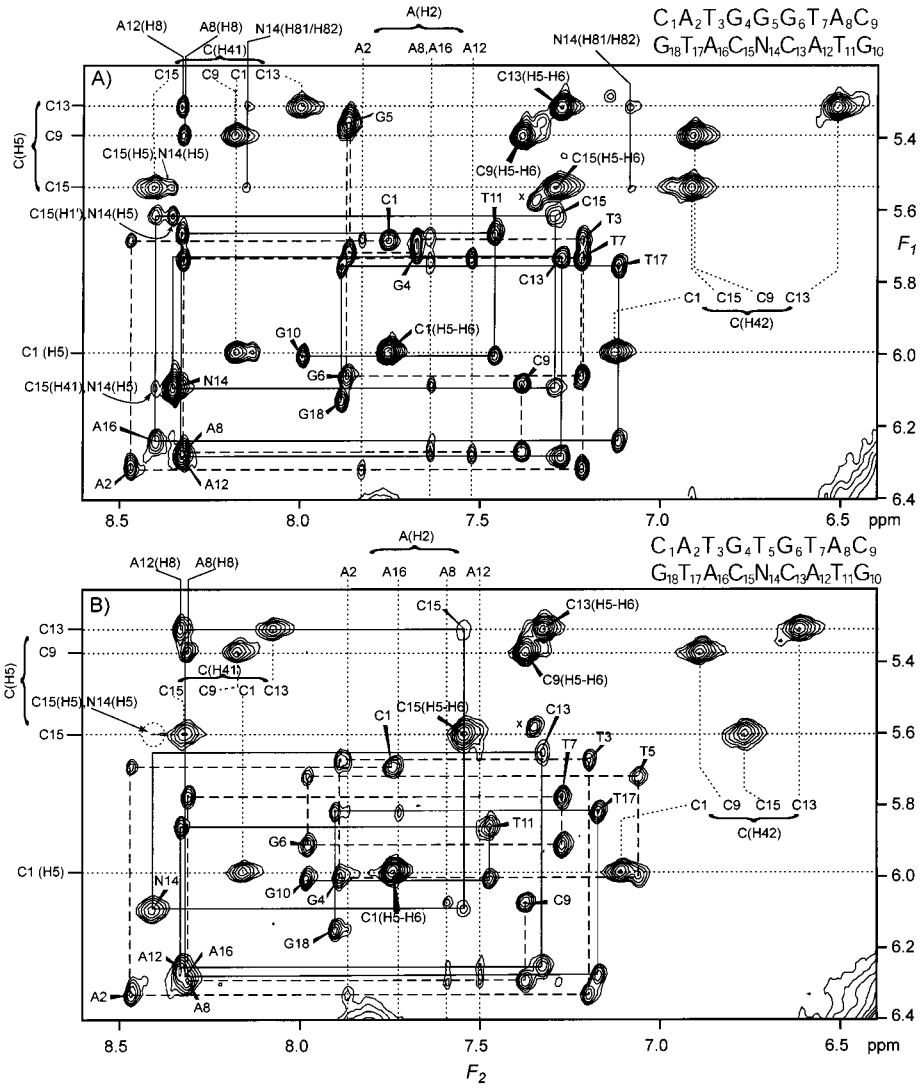

FIGURE 3: Contour plot of the aromatic (F_2) to H1′ (F_1) region of NOESY spectra (200 ms mixing time) of the duplexes recorded in 95% H_2O/5% D_2O at 5 °C; (A) duplex **1**, (B) duplex **2**. The solid and dashed lines follow the connectivity of the base protons through the H1′ sugar protons of the substituted and unsubstituted strands, respectively. The vertical dotted lines indicate the chemical shifts of the H2 protons of the adenines and the amide protons of the cytidines. The solid vertical lines correspond to the chemical shifts of the H8 protons of A8 and A12 and amide protons of **N**14. The horizontal dotted lines indicate the chemical shifts of the cytidine H5 protons. The x indicates an unassigned impurity that persists in the NOESY spectra of all of the duplexes studied (**1**−**4**).

protons (Figure 6), and had a wider line width than those of the other imino protons. This indicated that the T5 imino proton was more accessible for exchange with the solvent and/or experiencing line broadening by conformational exchange dynamics. The imino proton of T5 did have a weak cross-peak to the imino proton of G4, which established that the imino proton of T5 was positioned in the interior of the helix. Figure 6A shows that the imino proton of T5 also had a cross-peak with H5 of N14 and indicated that the H5 proton of the triazole ring was directed into the center of the helix.

DISCUSSION

The present studies were undertaken to determine how 1,2,4-triazole-3-carboxamide interacts with the opposite bases, G and T, and what perturbations it imparts to the DNA double helix. The thermodynamic and circular dichroism data revealed that **1** and **2** existed as B-form duplexes at ambient temperatures and with average conformations that were similar to but less stable than those of **3** and **4**, respectively (Figure 2). Therefore, the perturbations imparted by **N** were short range and did not have a significant effect on the global conformation.

Thermodynamic measurements showed that **1** was more stable than **2**. Earlier, Pochet and Duguè (*19*) also showed that G:**N** is a more stable base pair than T:**N**. However, our results showed that the $\Delta\Delta G^\circ_{25}$ for **1** to **3** was the same as the $\Delta\Delta G^\circ_{25}$ for **2** to **4** (Table 1). Thus, the difference in stability between **1** and **2** was not due to a difference between the stabilities of the G5:**N**14 and T5:**N**14 base pairs. Instead, the poorer base stacking of G4-T5-G6 in **2** relative to that of G4-G5-G6 in **1**, independent of **N**, was most likely responsible for the measured differences in stability.

On the basis of models and the duplex melting studies, we first hypothesized that **N**14:G5 and **N**14:T5 would be particularly stable because the modified nucleoside would adopt conformations in which there could be two hydrogen bonds to the natural bases (Figure 1). In this arrangement, the values of two key geometric parameters, C1′ to C1′ distance and angles θ_1 and θ_2 (Figure 1), would closely match the values found in natural base pairs. Molecular models

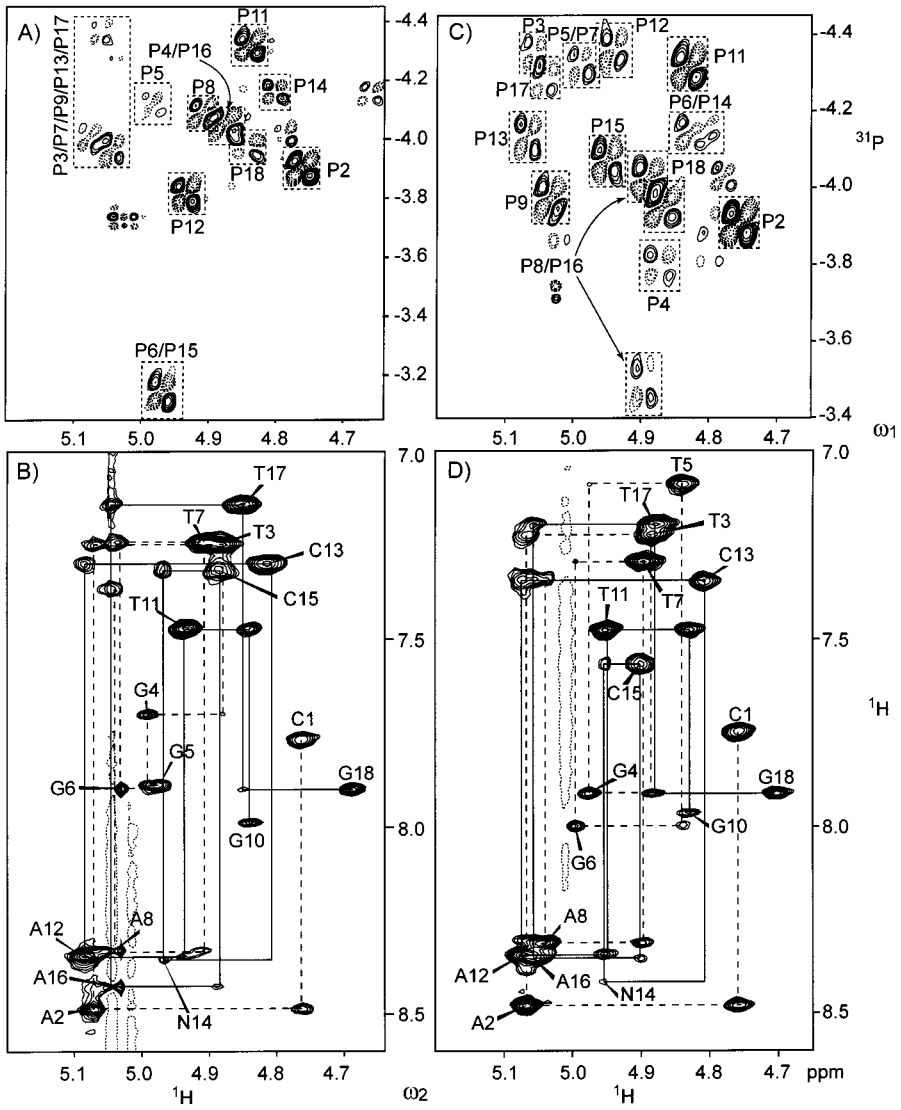

FIGURE 4: Expanded contour plots of the two-dimensional ^{1}H-^{31}P correlation spectra (A, C) and base-to-H3′ region (B, D) of the two-dimensional NOESY spectra in D_2O for duplex **1** (A, B) and **2** (C, D). The dotted contours indicate negative intensities. The solid and dashed lines indicate the sequential assignments of the H3′ protons in the substituted and unsubstituted strands, respectively. Cross-peaks in panels A and C are between the H3′ proton of residue *i* and the phosphate of residue *i* + 1. Intraresidue cross-peaks in panels B and D are indicated by residue number. The negative contours in panels B and D are due to residual HDO.

showed that this was not possible for the base pairs with **N** opposite A or C. The NMR study was designed to test this hypothesis and, in doing so, provide a foundation for the design and application of the azole carboxamide family of modified nucleosides.

Glycosidic Bond Angle. The intensity of the cross-peak between a base proton and its own H1′ proton is an indicator of the torsion angle about the glycosidic bond, χ. If the base is in the syn conformation (Figure 1), the base proton is within 2.5 Å of its own H1′, and the intensity of the corresponding cross-peak would be similar to that of the cross-peak between cytidine H5−H6 protons, which are 2.45 Å apart (*28*). Conversely, if the χ angle of the base is in the anti conformation, the base proton is farther away from its own H1′ (about 3.7 Å in A- and B-form duplexes) and the intensity of the corresponding cross-peak would be significantly reduced. Thus, the intensities of the base to H1′ cross-peaks indicated that all of the χ angles in both **1** and **2**, with the exception of **N**14, were in the anti conformation. Although the cross-peak labeled G5 in Figure 3A was composed of two degenerate cross-peaks, it was possible to determine that the conformation of the χ angle of G5 was anti. There were cross-peaks between the H8 of G5 and the H1′ of G4 (Figure 3A) and between the imino proton of G5 and the amino protons of C13 (Figure 5A), both of which would be difficult to observe if the χ angle of G5 was syn. Furthermore, the total integrated intensity of the overlapped peaks of G5 was only 56% of those of the cross-peaks between the H5 and H6 protons of the cytidines.

The integrated volume of the intraresidue NOESY cross-peak between H5 and H1′ of **N**14 in **1** was 97% of the average of the volumes of the intraresidue cross-peaks between the H5 and H6 protons of the cytosine residues. In addition, there was no observable cross-peak between H5 of **N**14 and H1′ of C13 (Figure 3A) and a weak cross strand cross-peak between H5 of **N**14 and the imino proton of G5 (Figure 5). These data indicated that the χ angle of **N**14 of **1** was, on average, in the syn conformation. Similarly, in the NOESY spectrum of **2** there was no observable cross-peak between H5 of **N**14 and H1′ of C13 (Figure 3B) and a weak interstrand cross-peak between H5 of **N**14 and the imino proton of T5 (Figure 6). These data indicated that the

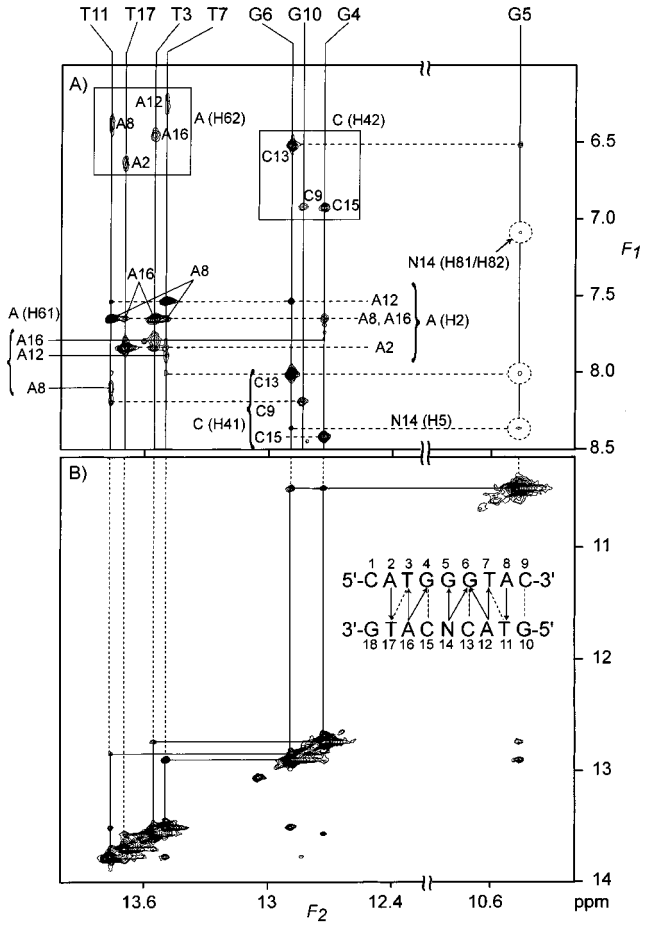

FIGURE 5: Expanded regions of contour plots of the imino proton region of the two-dimensional NOESY spectrum (200 ms mixing time) of **1** in 95% H_2O/5% D_2O at 5 °C. (A) Cross-peaks between imino and inter- and intrastrand base protons. (B) Symmetrical region showing cross-peaks between imino protons and the sequential assignment of the imino protons along the length of the duplex. The DNA sequence is shown in panel B and the arrows and dashed lines correspond to interstrand NOEs between H2 protons of adenine and imino protons of thymidine and guanosine and between amino protons of cytidine and imino protons of guanosine, respectively.

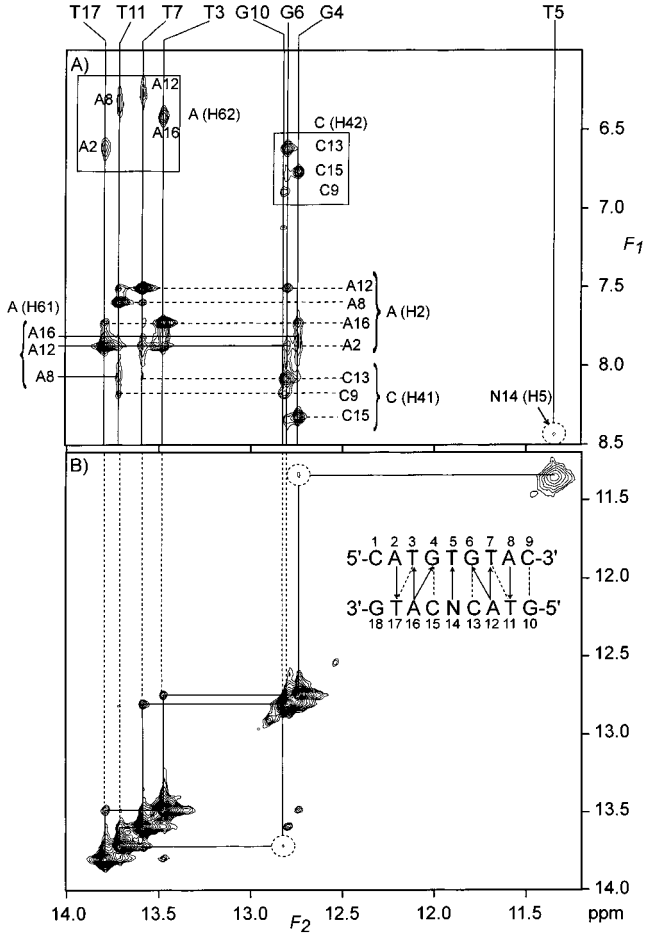

FIGURE 6: Expanded regions of contour plots of the imino proton region of the two-dimensional NOESY spectrum (200 ms mixing time) of **2** in 95% H_2O/5% D_2O at 5 °C. (A) Cross-peaks between imino and inter- and intrastrand base protons. (B) Symmetrical region showing cross-peaks between imino protons and the sequential assignment of the imino protons along the length of the duplex. The DNA sequence is shown in panel B and the arrows and dashed lines correspond to interstrand NOEs between H2 protons of adenine and imino protons of thymidine and guanosine and between amino protons of cytidine and imino protons of guanosine, respectively.

χ angle of **N**14 of **2** was also in the syn conformation on average. However, the line widths of H5 of **N**14 were relatively broad and the intensity of the intraresidue NOESY cross-peak between H5 and H1′ of **N**14 in **2** was only 57% of that of the intraresidue cross-peak between H5 and H6 of the C15. These data suggest that **N**14 of **2** was experiencing conformational exchange broadening. These results were surprising because it was predicted that hydrogen bonding with the opposing base would drive the triazole ring to undergo a 180° rotation about the glycosidic bond when pairing with T versus G and **N**14 would be in the anti$_\chi$ or syn$_\chi$ conformations, respectively (Figure 1) (*15*). Instead, **N**14 was observed to adopt the syn$_\chi$ conformation in both **1** and **2**.

Amide Conformation of N14. Assignment of the individual amide protons of **N**14 was not possible with the present data. In the absence of hydrogen bond formation, the proton cis to the carbonyl would be deshielded relative to the trans proton by the anisotropy of the carbonyl bond (*29*). Thus, the resonances at 8.16 and 7.10 ppm of duplex **1** would be assigned to the cis and trans protons, respectively. However, if the trans proton was involved in a hydrogen bond, its resonance could be shifted to higher frequency and could potentially reverse the assignment (*30*). It was not necessary to assign each of these protons to make conclusions about the conformation of the amide group in general.

The NMR data supported a structure in which the triazole base of **1** was in the syn$_\chi$ conformation. The carboxamide group of the triazole ring would then be projecting out of the DNA double helix into the major groove regardless of whether τ was syn or anti. The amide protons of **N**14 were observed to have weak NOEs with the H5 protons of C13 and C15 (Figure 3) and with the imino proton of G5 (Figure 5). However, in models of ideal B-form DNA with the triazole base fixed in the syn$_\chi$ conformation, the amide protons of **N**14 did not approach within 5 Å of the H5 of C15 when τ was syn or anti (Figure 7), which was inconsistent with the NOESY data. The same models showed that rotation about τ would bring the amide protons of **N**14 as close as 3.8 Å from the H5 protons of C15. Therefore, the presence of NOEs between the amide protons of **N**14 and the H5 protons of C13 and C15 would be consistent

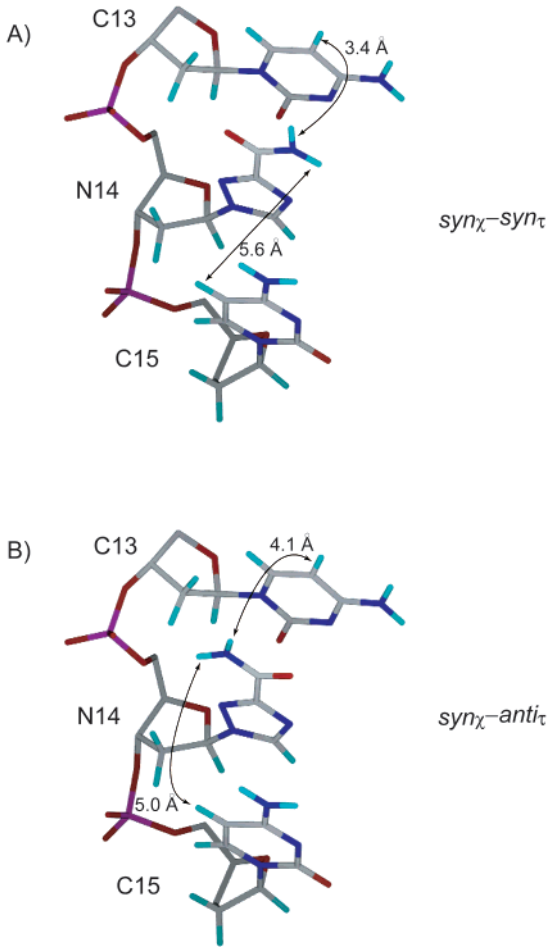

FIGURE 7: Models of ideal B-form DNA of C13, **N**14, and C15 with the χ and τ angles of **N**14 in the (A) syn$_\chi$ and syn$_\tau$ and (B) syn$_\chi$ and anti$_\tau$ conformations, respectively. Carbon is colored gray, oxygen is red, hydrogen is light blue, nitrogen is dark blue, and phosphorus is purple. Distances between the amino protons of N14 and the H5 protons of C13 and C15 are indicated.

with conformational exchange about τ which was slow on the NMR time scale. Alternatively, if τ was fixed at −60° [-synclinal (*24*)] the amide protons of **N**14 would be 4.3 Å from the H5 protons of C13 and C15 (Supporting Information) and would produce NOEs that were also consistent with our NOESY spectra. There were no resonances in the NMR spectra of **2** that could be attributed to the amide protons of **N**14. This suggested that there was conformational exchange about τ on the intermediate time scale and/or the amide protons of **N**14 were subject to rapid exchange with the solvent.

Base Pairing. Watson−Crick base pairing was established in A:T base pairs in duplexes **1**−**4** by the observation of NOESY cross-peaks between each thymidine imino proton and the H2 and amino protons of the opposing adenosine (Figures 5 and 6). Similarly, Watson−Crick base pairing of all G:C base pairs except C1:G18 were established by the observation of NOESY cross-peaks between the guanosine imino proton and the amino protons of the cytidine. Thus, the base pairs that flank the center X5:**N**14 base pair, G4:C15 and G6:C13, were not disrupted in **1** and **2**. A weak NOE between H5 of **N**14 and the imino proton of the opposing base of **1** and **2** indicated that the aromatic rings of each X5:**N**14 base pair were directed toward each other and were located in the interior of the helix. In duplexes **1** and **2**, the chemical shifts of the imino protons of both G5 and T5 were shifted 3−3.5 ppm to lower frequency compared to the other hydrogen-bonded imino protons (Figures 5 and 6). Their chemical shifts suggested that the imino protons of G5 and T5 were either not hydrogen bonded or hydrogen bonded weakly with the ring nitrogens (or oxygen of the carboxamide) of **N**14.

Table 2: Total Energies (Hartrees), Relative Energies (kcal/mol), and Dipole Moments (μ, D) for anti$_\tau$ and syn$_\tau$ Conformations of 1-Methyl-1,2,4-triazole-3-carboxamide[a]

	6-31G(d,p), $\epsilon = 1$			6-31G(d,p), $\epsilon = 40$		
	$E_{SCF(rel)}$	E_{SCF}	dipole moment	$E_{SCF(rel)}$	E_{SCF}	dipole moment
anti$_\tau$	0.00	−450.28	6.57	−2.61	−450.30	8.00
syn$_\tau$	−1.58	−450.28	5.26	0.00	−450.29	6.33

[a] All calculations were carried out with the Gaussian 94 software package using density functional theory with the 6-31G(d,p) basis set. The self-consistent reaction field (SCF) was used to calculate the solvation medium effect (*15*).

Hydrogen Bonding of G5 and T5. Previous studies on DNA duplexes with sheared G:A pairs have shown that the non-hydrogen-bonded imino proton of the guanosines resonated at approximately 10.5 ppm (*31*, *32*). On the other hand, hydrogen-bonded imino protons of guanosines in G:U base pairs in RNA duplexes also resonate around 10.5 ppm (*33*). Others have shown that the chemical shift of an imino proton of a guanosine base was 10.2 ppm when hydrogen bonded to the oxygen of a formamide group in a DNA duplex containing a formamide lesion (*34*). Thus, a chemical shift of 10.5 ppm for the imino proton of a guanosine base can be due to the absence of a hydrogen bond or the nature of the hydrogen bond acceptor. Upon the basis of these previous findings, the imino proton of G5 of **1** could have either been non-hydrogen bonded or weakly hydrogen bonded with the carbonyl oxygen of the carboxamide group of **N**14. In either case, the relatively broad line widths of the imino proton of G5 (Figure 5) suggested that it was exchanging with solvent at an increased rate. The imino proton of T5 of **2** had a similarly upfield shifted resonance and relatively broad line width (Figure 6) and suggested that it too was either not hydrogen bonded or only weakly hydrogen bonded.

Energy Calculations. We have carried out calculations on the model compound 1-methyl-1,2,4-triazole-3-carboxamide to determine the relative preferences of τ (Figure 1). We used the Density Functional Theory (DFT) method, B3LYP (*35*−*38*) with the basis set 6-31G(d,p) to calculate energies in the gas phase and a self-consistent reaction field (SCRF) method to study solvent medium effects (*39*−*41*) as previously described for the theoretical analysis of 1-methylpyrrole-3-carboxamide (*15*). The results of the DFT calculation are summarized in Table 2. In the gas phase (dielectric constant, $\epsilon = 1$), anti$_\tau$ was more stable than syn$_\tau$ by 1.6 kcal/mol. As the polarity of the medium was increased, the difference in energy between the two conformers changed. At the highest polarity examined ($\epsilon = 40$), the syn$_\tau$ conformation was found to be more stable by 2.6 kcal/mol. The polarity inside the helix is expected to be somewhere between these two extremes (*15*). AM1 level calculations indicated that the barrier to rotation around τ was small (<1 kcal/mol). In comparison, two related azole carboxamides either showed a barrier to rotation (pyrrole-3-carboxamide

> 3 kcal/mol) or a significantly larger difference in energy between the two conformers (imidazole-4-carboxamide > 6 kcal/mol), which indicated that these other azole bases had a preferred conformation. However, for triazole-3-carboxamide, the above calculations were consistent with a duplex structure in which there was conformational exchange about τ between syn and anti. Our data suggested that it was likely that conformational exchange about τ occurred in both **1** and **2**. It should be mentioned that in the syn_χ−$anti_\tau$ conformation, the amide protons of **N**14 could come within 3.1 Å of the oxygens of the 5′ phosphate, form a hydrogen bond, and thereby bias **N**14 toward this conformation (*42*).

Backbone Conformation. The phosphorus spectra of **1** and **2** showed that the **N**14−P15−C15 (or G5-P6-G6) phosphate of **1** and the C15−P16−A16 (or T7−P8−A8) phosphate of **2** had downfield-shifted ^{31}P chemical shifts compared to the rest of the backbone phosphates. The P15 (or P6) phosphate of **1** was shifted about 0.8 ppm downfield from the other phosphates and the P16 (or P8) of **2** was shifted about 0.5 ppm downfield. Since P8 was located far away from **N**14, the perturbed phosphorus chemical shift most likely belonged to P16. In **1**, on the other hand, the downfield phosphate resonance could have belonged to either P15 or P6. DNA duplexes that contain G:A mismatches have been shown to have higher energy B_{II} conformations of the phosphates near the mismatched residues (*43*). The chemical shifts of the phosphates involved in the higher energy conformations were shifted downfield as much as 2 ppm. Studies of a DNA duplex with an abasic site showed that the phosphates that flank the abasic residue were shifted about 0.5−1.2 ppm downfield (*44*, *45*). On the basis of the $J_{H3'-P}$ coupling constants the ϵ torsion angles of the shifted phosphates were within the *anti*$^+$(+*ac*)/*anti*$^-$(-*ac*) ranges (*45*). In other words, the phosphates that flanked the abasic site, although shifted downfield, were still in the lower energy B_I conformation. In turn, because the downfield shifts of the phosphates in **1** and **2** were equally small, they were probably the result of small, localized perturbations in a B_I backbone.

SUMMARY

The NMR study provided a means to probe the conformational preferences of the 1,2,4-triazole-3-carboxamide nucleoside in different DNA sequence contexts. To serve as an A mimic in a base pair with T, triazole-3-carboxamide was expected to adopt the $anti_\chi$-syn_τ conformation (Figure 1). Contrary to expectations, our experimental results on **2** showed instead that the triazole existed in the syn_χ conformation and that the carboxamide was most likely experiencing conformational exchange on the intermediate time scale. The smaller size of the pyrimidine of T5 relative to the purine of G5 may have provided τ of **N**14 of **2** with more degrees of freedom and/or increased access to the solvent. To function as a C mimic in a base pair with G, triazole-3-carboxamide was expected to adopt the syn_χ-syn_τ conformation. However, the results on **1** showed that the carboxamide group of **N**14 existed in at least two conformational populations.

The projection of the carboxamide into the major groove requires that the glycosidic bond be in the syn_χ conformation. The preference for the syn_χ conformation in both duplexes (containing either G or T opposite the triazole-3-carboxamide) may have been influenced by the high polarity of the carboxamide group. The major groove presents a more hydrophilic environment than the interior of the helix and more effective solvation occurs when the carboxamide projects into this region. These insights into the structural influences on DNA conformation will contribute to our ability to design additional natural base surrogates for use as tools in molecular biology.

ACKNOWLEDGMENT

The authors would like to gratefully acknowledge Jon Christopher for help with the program Spock; David Giedroc and Paul Nixon for helpful discussions and help with the acquisition of the thermodynamic data; and Frank Delaglio, Dan Garrett, and Thomas Goddard for providing the NMR software. We are also thankful to J. Martin Scholtz and Ron Peterson for assistance with the acquisition of the circular dichroism data.

SUPPORTING INFORMATION AVAILABLE

There are three figures and two tables of ^{1}H chemical shift assignments. The figures include van't Hoff plots, one-dimensional ^{31}P spectra, and a figure of C13, N14, and C15 in the ideal B-form conformation and with the τ angle of N14 in the -*sc* conformation. This material is available free of charge via the Internet at http://pubs.acs.org.

REFERENCES

1. Hill, F., Loakes, D., Smith, C. L., Williams, D. M., and Brown, D. M. (1999) *Nucleosides Nucleotides 18*, 573−574.
2. Hill, F., Loakes, D., and Brown, D. M. (1998) *Proc. Natl. Acad. Sci. U.S.A. 95*, 4258−4263.
3. Hoops, G. C., Zhang, P. M., Johnson, W. T., Paul, N., Bergstrom, D. E., and Davisson, V. J. (1997) *Nucleic Acids Res. 25*, 4866−4871.
4. Bergstrom, D. E., Zhang, P., and Johnson, W. T. (1997) *Nucleic Acids Res. 25*, 1935−1942.
5. Bergstrom, D. E., Zhang, P. M., Toma, P. H., Andrews, P. C., and Nichols, R. (1995) *J. Am. Chem. Soc. 117*, 1201−1209.
6. Loakes, D., Brown, D. M., Linde, S., and Hill, F. (1995) *Nucleic Acids Res. 23*, 2361−2366.
7. Vanaerschot, A., Rozenski, J., Loakes, D., Pillet, N., Schepers, G., and Herdewijn, P. (1995) *Nucleic Acids Res. 23*, 4363−4370.
8. Loakes, D., and Brown, D. M. (1994) *Nucleic Acids Res. 22*, 4039−4043.
9. Nichols, R., Andrews, P. C., Zhang, P., and Bergstrom, D. E. (1994) *Nature 369*, 492−493.
10. Schweitzer, B. A., and Kool, E. T. (1995) *J. Am. Chem. Soc. 117*, 1863−1872.
11. Klewer, D. A., Hoskins, A., Zhang, P., Davisson, V. J., Bergstrom, D. E., and LiWang, A. C. (2000) *Nucleic Acids Res. 28*, 4514−4522.
12. Natasha, P., Hoops, G. C., Bergstrom, D. E., and Davisson, V. J. (1998) *FASEB J. 12*, 257.
13. Bergstrom, D. E., Zhang, P. M., Johnson, W. T., Klewer, D., Paul, N., Hoops, G. C., and Davisson, V. J. (1997) *FASEB J 11*, 2742.
14. Hoops, G. C., Zhang, P. M., Johnson, W. T., Paul, N., Chen, X. M., Bergstrom, D. E., and Davisson, V. J. (1997) *FASEB J 11*, 3005.
15. Zhang, P. M., Johnson, W. T., Klewer, D., Paul, N., Hoops, G., Davisson, V. J., and Bergstrom, D. E. (1998) *Nucleic Acids Res. 26*, 2208−2215.
16. Johnson, W. T., Zhang, P. M., and Bergstrom, D. E. (1997) *Nucleic Acids Res. 25*, 559−567.

17. Hoops, G. C., Zhang, P. M., Johnson, T. W., Bergstrom, D. E., and Davisson, V. J. (1996) *FASEB J. 10*, 725−725.
18. Bergstrom, D. E., Zhang, P. M., and Johnson, W. T. (1996) *Nucleosides Nucleotides 15*, 59−68.
19. Pochet, S., and Dugue, L. (1998) *Nucleosides Nucleotides 17*, 2003−2009.
20. Theimer, C. A., Wang, Y., Hoffman, D. W., Krisch, H. M., and Giedroc, D. P. (1998) *J. Mol. Biol. 279*, 545−564.
21. Wang, A. C., Kennedy, M. A., Reid, B. R., and Drobny, G. P. (1992) *J. Am. Chem. Soc. 114*, 6583−6585.
22. Sklenar, V., Piotto, M., Leppik, R., and Saudek, V. (1993) *J. Magn. Reson. Ser. A 102*, 241−245.
23. Sklenar, V., Miyashiro, H., Zon, G., Miles, T. H., and Bax, A. (1986) *Fed. Eur. Biochem. Soc. 208*, 94−98.
24. Markley, J. L., Bax, A., Arata, Y., Hilbers, C. W., Kaptein, R., Sykes, B. D., Wright, P. E., and Wüthrich, K. (1998) *Pure Appl. Chem. 70*, 117−142.
25. Hare, D. R., Wemmer, D. E., Chou, S.-H., Drobny, G., and Reid, B. R. (1983) *J. Mol. Biol. 171*, 319−336.
26. Weiss, M. A., Patel, D. J., Sauer, R. T., and Karplus, M. (1984) *Proc. Natl. Acad. Sci. U.S.A. 81*, 130−134.
27. Feigon, J., Leupin, W., Denny, W. A., and Kearns, D. R. (1983) *Biochemistry 22*, 5943−5951.
28. Wuthrich, K. (1986) *NMR of Proteins and Nucleic Acids*, John Wiley & Sons, New York.
29. Stewart, W. E., and Siddall, T. H. (1970) *Chem. Rev. 70*, 517−551.
30. Klewer, D. A. (1998) *^{1}H NMR Study of the Hydrogen Bonding of Modified Nucleosides* (Ph.D. Thesis), Purdue University, West Lafayette, IN.
31. Chou, S.-H., Cheng, J.-W., and Reid, B. (1992) *J. Mol. Biol. 228*, 138−155.
32. Li, Y., Zon, G., and Wilson, W. D. (1991) *Proc. Natl. Acad. Sci. U.S.A. 88*, 26−30.
33. Addess, K. J., Basilion, J. P., Klausner, R. D., Rouault, T. A., and Pardi, A. (1997) *J. Mol. Biol. 274*, 72−83.
34. Maufrais, C., Fazakerley, G. V., Cadet, J., and Boulard, Y. (2000) *Biochemistry 39*, 5614−5621.
35. Becke, A. D. (1988) *Phys. Rev. A 38*, 3098−3100.
36. Becke, A. D. (1993) *J. Chem. Phys. 98*, 5648−5652.
37. Lee, C., Yang, W., and Parr, R. G. (1988) *Phys. Rev. B 37*, 785−789.
38. Vosko, S. H., Wilk, L., and Nusair, M. (1980) *Can. J. Phys. 58*, 1200.
39. Tapia, O., and Goscinski, O. (1975) *Mol. Phys. 29*, 1653−1661.
40. Wong, M. W., Frisch, M. J., and Wiberg, K. B. (1991) *J. Am. Chem. Soc. 113*, 4776−4782.
41. Onsager, L. (1936) *J. Am. Chem. Soc. 58*, 1486-1493.
42. Vijayaiakshmi, K. S., and Yathindra, N. (1980) *Biochim. Biophys. Acta 607*, 171−186.
43. Chou, S.-H., Cheng, J.-W., Fedoroff, O. Y., Chuprina, V. P., and Reid, B. R. (1992) *J. Am. Chem. Soc. 114*, 3114−3115.
44. Kalnik, M. W., Chang, C.-N., Johnson, F., Grollman, A. P., and Patel, D. J. (1989) *Biochemistry 28*, 3373−3383.
45. Lin, Z., Hung, K.-N., Grollman, A. P., and Santos, C. (1998) *Nucleic Acids Res. 26*, 2385−2391.
46. SantaLucia, J., Jr., and Turner, D. H. (1997) *Biopolymers 44*, 309−319.

BI001448F